remote sensing

MDPI

Article

Low-Frequency Ground Penetrating Radar for Active Fault Characterization: Insights from the Southern Apennines (Italy)

Nicola Angelo Famiglietti [1,*], Gaetano Memmolo [1], Antonino Memmolo [1], Robert Migliazza [1], Nicola Gagliarde [2], Daniela Di Bucci [3], Daniele Cheloni [4], Annamaria Vicari [1] and Bruno Massa [2]

1 Sezione Irpinia, Istituto Nazionale di Geofisica e Vulcanologia, 83035 Grottaminarda, Italy; gaetano.memmolo@ingv.it (G.M.); antonino.memmolo@ingv.it (A.M.); robert.migliazza@ingv.it (R.M.); annamaria.vicari@ingv.it (A.V.)
2 Dipartimento di Scienze e Tecnologie, Università Degli Studi del Sannio, 82100 Benevento, Italy; n.gagliarde1@studenti.unisannio.it (N.G.); massa@unisannio.it (B.M.)
3 Dipartimento della Protezione Civile, 00131 Rome, Italy; daniela.dibucci@protezionecivile.it
4 Osservatorio Nazionale Terremoti, Istituto Nazionale di Geofisica e Vulcanologia, 00143 Rome, Italy; daniele.cheloni@ingv.it
* Correspondence: nicola.famiglietti@ingv.it

Highlights

What are the main findings?

- The integration of GPR data with precise georeferencing is effective in providing new constraints on the geometry and kinematics of shallow active faults in sedimentary deposits.
- In the case study area, the Calore River Valley (Southern Apennines), low-frequency GPR imaging revealed steeply dipping E–W to ENE–WSW normal faults, consistent with an active system, named Postiglione Fault System.

What is the implication of the main finding?

- The results demonstrate the potential of low-frequency GPR to resolve near-surface fault architecture where surface evidence is scarce or ambiguous.
- These findings also contribute to refining the seismotectonic framework of the Southern Apennines, supporting improved seismic hazard assessment in one of the most seismically active regions of the Mediterranean.

Abstract

Ground Penetrating Radar (GPR) is a powerful tool for imaging shallow stratigraphic and structural features. This study shows that it is particularly effective also in detecting near-surface evidence of active faulting. In the Southern Apennines (Italy), one of the most seismically active regions of the Mediterranean area, the shallow expression of active faults is often poorly constrained due to limited or ambiguous surface evidence. Low-frequency GPR profiles were acquired in the Calore River Valley (Campania Region), an area historically affected by large earthquakes and characterized by debated seismogenic sources. The surveys employed multiple antenna frequencies (30, 60, and 80 MHz) and both horizontal and vertical acquisition geometries, enabling penetration depths ranging from ~5 m to ~50 m. The acquired GPR profiles, integrated with high-precision georeferencing, were able to reveal the presence of shallow steeply dipping active normal faults striking E–W to ENE–WSW, here named the Postiglione Fault System. Therefore, this study highlights the methodological potential of low-frequency GPR for investigating active faults in carbonate substratum and fine-to-coarse-grained sedimentary units and thus contributing to refining the seismotectonic framework and improving seismic hazard assessment of seismically active areas such as the Southern Apennines.

check for updates

Academic Editors: Pietro Tizzani, Daniele Cirillo and Francesco Brozzetti

Received: 27 September 2025
Revised: 31 October 2025
Accepted: 1 November 2025
Published: 3 November 2025

Citation: Famiglietti, N.A.; Memmolo, G.; Memmolo, A.; Migliazza, R.; Gagliarde, N.; Di Bucci, D.; Cheloni, D.; Vicari, A.; Massa, B. Low-Frequency Ground Penetrating Radar for Active Fault Characterization: Insights from the Southern Apennines (Italy). *Remote Sens.* **2025**, *17*, 3631. https://doi.org/10.3390/rs17213631

Copyright: © 2025 by the authors. Licensee MDPI, Basel, Switzerland. This article is an open access article distributed under the terms and conditions of the Creative Commons Attribution (CC BY) license (https://creativecommons.org/licenses/by/4.0/).

Keywords: Ground Penetrating Radar (GPR); active tectonics; Calore River Valley; Southern Apennines; Postiglione Fault System; earthquake geology

1. Introduction

In recent years, in situ geophysical methods have become increasingly important tools for subsurface investigations, owing to their efficiency, cost-effectiveness, and capacity to provide high-resolution images in a non-invasive approach. Among these, Ground Penetrating Radar (GPR) has emerged as one of the most versatile techniques for shallow subsurface imaging, typically reaching depths of several tens of meters. Its applications span a broad spectrum of disciplines, ranging from environmental and engineering studies to geological and structural investigations [1–5]. Over the last decades, GPR has been successfully applied in various geological settings, including sedimentary successions and slope deposits affected by gravity-driven mass movements, consistently demonstrating its ability to resolve structural and stratigraphic features with decimetric precision [6–8].

In tectonically active regions, the characterization of shallow fault geometries and recent surface deformation typically requires a multidisciplinary approach combining paleoseismological trenching, structural field surveys, geomorphological analysis, remote sensing, and geophysical techniques, such as seismological monitoring and geodetic observations [9–11]. While these methods provide fundamental insights for characterizing fault activity, they are not always feasible: trenching is site-specific, invasive and costly, and surface observations may be hindered by erosion, anthropogenic overprint, or the absence of clear geomorphic markers. In this context, GPR can represent an effective alternative, offering a rapid, low-cost, and non-invasive approach to detect subtle deformation features and constrain the near-surface expression of active faults.

This study aims to explore the potential of this methodology in defining active faults in mountain areas. To do this, the Calore River Valley (Campania region, Southern Italy), located across the Apennines chain axis in the Sannio–Matese Domain (Figure 1), was selected as a case study area.

Instrumental seismicity in this area shows an overall low-energy activity (Figure 1). Activity at Sannio–Matese Domain in recent decades mainly consisted of isolated events with $M_L < 3.0$ and hypocentral depth up to 20 km [12–14]. Low and moderate magnitude seismic sequences and swarms also occurred, such as the 2013–2014 Matese sequence ($M_L \leq 5.0$, [15]) and the 1997–1998, 1999, 2000, 2001, 2005 sequences ($M_L \leq 4.0$, [14]).

The Parametric Catalogue of Italian Earthquakes [16,17], however, documents several destructive seismic events in this area, with magnitudes up to Mw ~7, associated with NW–SE and nearly E–W striking faults [12]. In the shallow crust, the prevailing stress field in this area is characterized by an extensional regime (NE–SW horizontal σ_3 and subvertical σ_1), which favors the activity of normal faults down to 10–12 km depth [18–20]. At greater depths, principal stresses rotate toward a strike-slip regime, with sub-horizontal σ_1 and σ_3, generating deep-seated seismicity associated with strike-slip kinematics [21,22].

In detail, the historical seismic record of this region includes a series of catastrophic earthquakes (Figure 1) such as the 1456 (Mw 7.19) and 1805 (Mw 6.68) Molise events, the 1688 (Mw 7.06) Sannio, the 1732 (Mw 6.75) and 1980 (Mw 6.9) Irpinia, and the 1857 (Mw 7.12) Basilicata earthquakes, all of which released high seismic moment and were associated with regional extension rates up to ~3.2 mm/yr [23–26]. For several of these events, the causative structures have been identified: the 1980 Irpinia earthquake has been related to a segmented NW–SE striking normal fault system [27], the 1857 Basilicata event to a similarly oriented extensional source [28,29], while the 1805 Molise earthquake is

interpreted to be associated with the Bojano Basin Fault System, a NE-dipping normal fault documented through field observations and paleoseismological analyses [30].

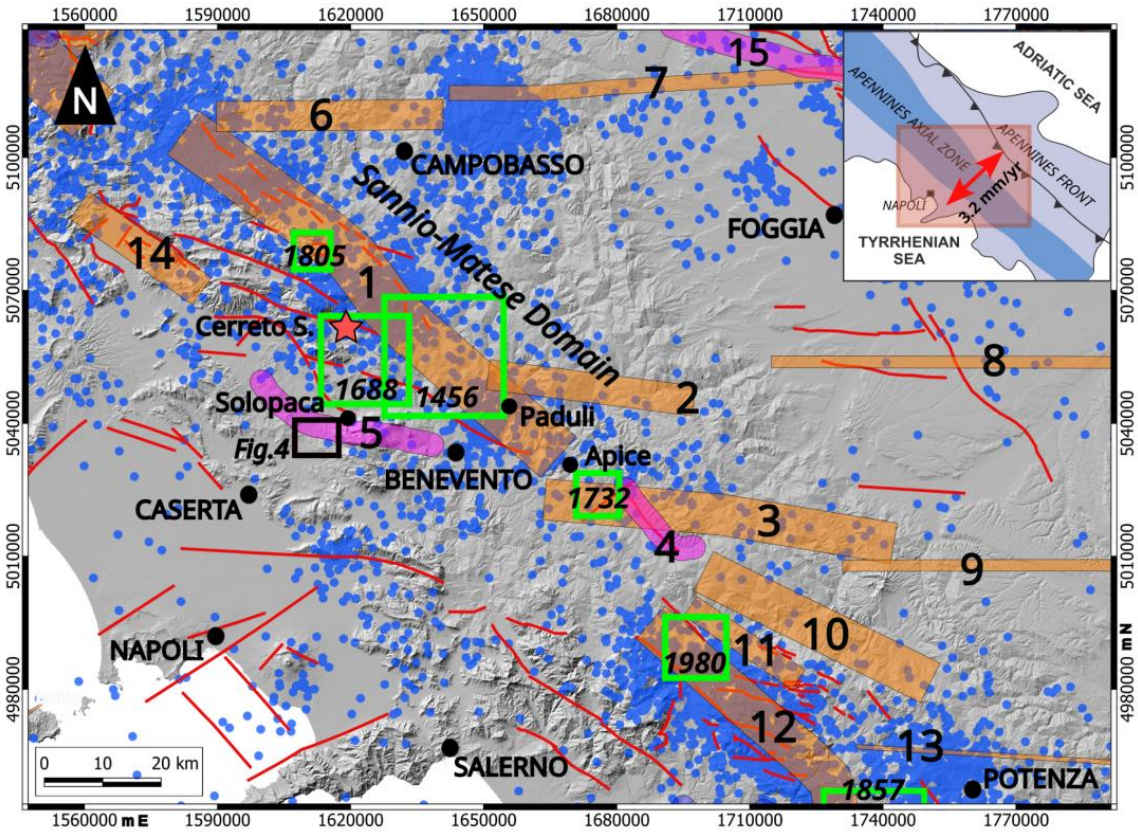


Figure 1. Map of the Southern Apennines Seismogenic Sources (DISS 3.3.1, DISS working Group, 2025 [12]) integrated with the Italy Hazards from Capable faults (red lines) catalogue (ITHACA, ISPRA). The orange boxes represent the Individual Seismogenic Sources: Miranda–Apice (1), Pago Veiano–Montaguto (2), Mirabella Eclano–Monteverde (3), Pescolanciano–Montagano (6), Ripabottoni–San Severo (7), Castelluccio dei Sauri–Trani (8), Rapolla–Spinazzola (9), Andretta–Filano (10), Conza della Campania–Tolve (11), Irpinia–Agri Valley (12), Baragiano–Palagianello (13), Venafro (14). Fuchsia strips represent the Debated Seismogenic Sources: Ufita Valley (4), Calore River (5), and Apricena (15). The black box represents the study area. The macroseismic epicenter of the 1688 Sannio earthquake is also reported (red star). Green squares represent hypocenters of some historical earthquakes (years in black), square dimension is proportional to $10^{\wedge}M_w/100{,}000$). The upper-right inset shows the regional tectonic setting, an average extension rate is also reported [25]. Blue dots are epicenters of 1990–2025 ($0 < M_L <$ Max) earthquakes (Istituto Nazionale di Geofisica e Vulcanologia, Creative Commons Attribution 4.0 International License. The Coordinate Reference System adopted for this figure is EPSG:3857-WGS 84/Pseudo-Mercator).

The 1688 Sannio earthquake, among the most destructive in Southern Apennines history [25], still raises debates about its causative structure. Different hypotheses have been proposed: (i) a 30 km-long SW-dipping normal fault between Cerreto Sannita and Paduli (Figure 1) [31]; (ii) a ~32 km WNW–ESE source inferred from the damage distribution [32]; (iii) a NW–SE trending normal fault dipping 60° toward NE, inferred from historical and geomorphological evidence [33]; (iv) an active fault system north of Mt. Camposauro, with NE-dipping geometry and a length of ~32 km [34]. More recently, based on surface geological data, some authors [35] suggested that the event originated from a 45 km-long fault system affecting the Calore River Valley between Apice and Solopaca, consisting of two E–W-oriented, NE-dipping segments linked by a N–S transfer zone near Benevento. However, the well-known E–W striking faults exposed in this area are inherited from

previous tectonic regimes, and only affect the shallowest thrust sheet of the fold-and-thrust belt [36], without reaching seismogenic depths.

Although several active faults have been mapped [37], the seismotectonic framework of the Calore R. Valley remains only partly resolved. Many sources are still poorly constrained, mainly where faults lack clear surface evidence [31,38–41]. In such cases, the detection of subtle surface deformation becomes crucial for reconstructing fault geometries and identifying hidden structures.

In this work, we propose the use of low-frequency Ground Penetrating Radar (GPR) to investigate near-surface deformation related to active faults in seismogenic regions. With this aim, we selected as a study area the western Calore R. Valley, where evidence of recent tectonic activity has been reported. While previous studies dated sedimentary deposits of this sector to 45 ka ± 5 [34], new chronologies suggest a younger age (<9 ka) [35], providing additional motivation for applying geophysical imaging techniques to this environment.

1.1. Geological Setting

The Calore River Valley is located in the Southern Apennines, a fold-and-thrust belt that has evolved since the Late Cretaceous as part of the Alpine–Mediterranean orogenic system [42]. Its structure reflects the tectonic superposition of two main paleogeographic domains: the Apennine Carbonate Platform, composed of Mesozoic limestones and dolostones, and the Lagonegro–Molise Pelagic Basin, made up of Cenozoic sediments including varicolored shales, marls, calcarenites, and breccias [43–45] (Figure 2).

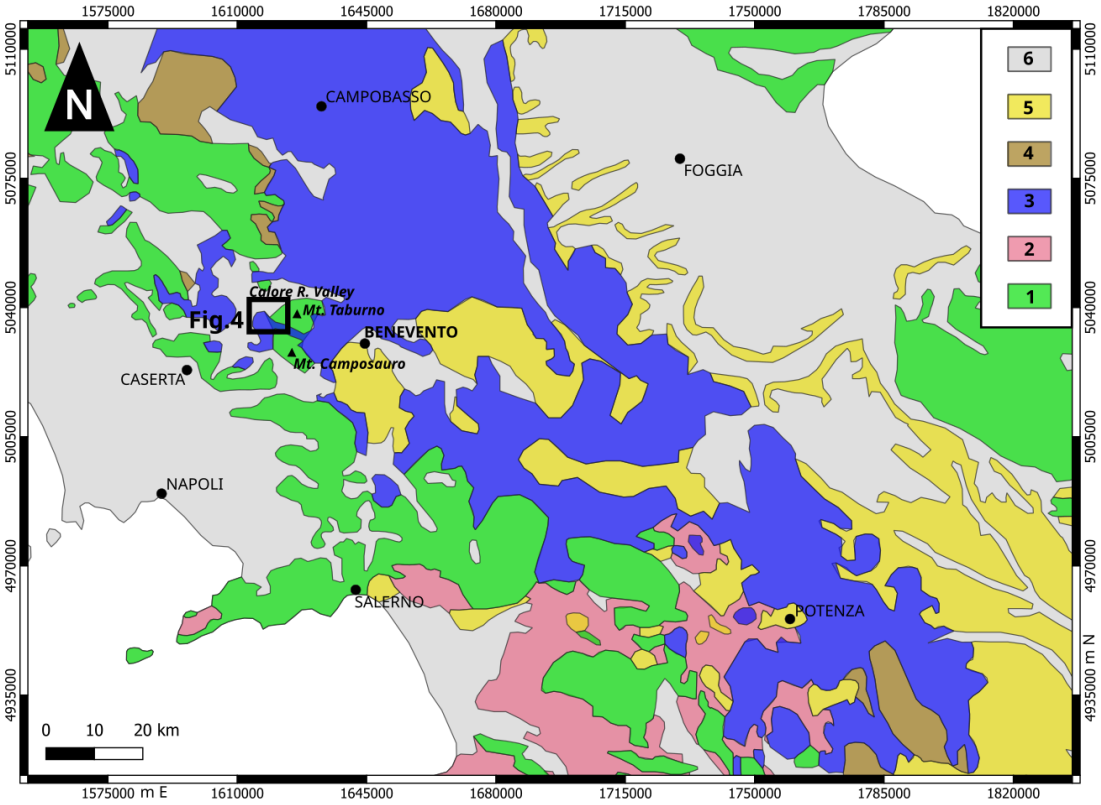


Figure 2. Schematic geological map of the Southern Apennines (modified from [46]), highlighting the location of the study area (black box,). 1. Apennine Carbonate Platform carbonates (Mesozoic); 2. Nord–Calabrese, Parasicilide and Sicilide Units (Meso-Cenozoic); 3. Lagonese–Molise–Sannio Basin Units (Cenozoic); 4. Wedge-top basin units (Miocene); 5. Wedge-top basin units (Pliocene–Quaternary); 6. Sedimentary and volcanic deposits (Quaternary).

Wedge-top basins units of Late Neogene age often occur at the top of these successions, frequently overlying thrust-sheet boundaries [47–50]. During the Miocene–Pliocene, the opening of the Tyrrhenian Basin accompanied the eastward propagation of the Apennine accretionary prism, with NE-verging thrusting active until the middle Pleistocene [51–54]. By the middle Pleistocene, the chain's axial sectors experienced a transition to extensional tectonics, driven by NE–SW extension [20,37,55–57]. Active normal and strike-slip faults partly reactivate pre-existing faults and thrust structures [36,37,58].

1.2. Stratigraphic Setting

The Quaternary deposits of the Calore R. Valley mainly consist of fluvial gravels interbedded with sandy–clayey lacustrine facies, forming a staircase of Pleistocene–Holocene terraces. These deposits are bordered by debris fans and talus slopes, mantling steep carbonate ridges and structural scarps. Travertine deposits occur near Telese town, where mineral waters record mantle degassing through anomalous $^{3}He/^{4}He$ values [59]. Widespread pyroclastic deposits, particularly the Campanian Ignimbrite (39 ka; [60]), provide chronological markers across the area. Five terrace orders (I–V) have been recognized:

- ***Terrace I*** (230–250 m a.s.l.): erosional surfaces carved into Mesozoic–Cenozoic bedrock, Middle Pleistocene in age (between ca. 680 and 240 ka).
- ***Terrace II*** (150–200 m a.s.l.): depositional gravels and lacustrine beds, capped by a pyroclastic layer dated between 158 $\pm$ 6 ka and 97 $\pm$ 25 ka.
- ***Terrace III*** (125–150 m a.s.l.): polygenic gravels overlain by the Campanian Ignimbrite (39 ka), dated between 48 $\pm$ 7 ka and 39 ka.
- ***Terrace IV*** (70–90 m a.s.l.): poorly cemented deposits, formed between 39 ka and <7 ka.
- ***Terrace V*** (50–70 m a.s.l.): Holocene terraces containing reworked pottery fragments, archeological evidence of Neolithic activity [61] and *Pomici di Avellino* eruption deposits that constrain them between ca. 14 ka and ca. 7 ka.

Debris fans, particularly near Solopaca, show two distinct generations: first-generation fans interfingered with Terrace IV deposits (between 39 ka and <7 ka) and second-generation fans unconformably overlain by Terrace V, pointing to early Holocene activity. This stratigraphic setting highlights the cyclic alternation of fluvial, volcanic, and tectonically controlled sedimentation shaping the Quaternary evolution of the valley [34,35,62].

1.3. Seismotectonic Setting

The Mediterranean basin hosts some of the most seismically active areas in Europe, primarily distributed along major mountain chains such as the Hellenic Arc, the Dinarides, the Alps, and the Apennines [63]. Within this geodynamic framework, Southern Italy represents one of the most active regions, with seismicity clustering along the axial sector of the Southern Apennines. The strongest historical earthquakes recorded in this region have been generated by fault systems aligned with the Apennine Chain ridge and its southern continuation into the Calabrian Arc. Historical epicenters are consistent with seismogenic structures reported in the DISS 3.3.1 database, confirming the structural control exerted by active, mainly normal faults [12,17,25,33,62,64–66].

The Sannio–Irpinia sector of the Southern Apennines hosts some key seismogenic sources, many of them described in the DISS 3.3.1 database. These include: (i) the Miranda–Apice system, comprising NE-dipping normal faults such as Carpino–Le Piane, Boiano, and Tammaro Basin; (ii) the Pago Veiano–Montaguto System, including the Ariano Irpino Fault, associated with right-lateral strike-slip kinematics; (iii) the Mirabella Eclano–Monteverde System, with the Ufita Valley and Bisaccia Faults, linked to transcurrent tectonics; and

(iv) the Benevento Mid-Crust Fault, a dextral strike-slip structure at ~15 km depth invoked to explain deep seismicity showing transcurrent kinematics [12,22,67].

Geodetic measurements indicate a complex kinematic pattern, with NE-directed motion in the eastern part of the Italian peninsula and NW to N-directed motion along the Tyrrhenian margin (INGV-RING GNSS Network [68]). Stress inversions from seismological data show prevailing NE–SW extension, up to about 12–15 km depth, but local stress variations are also observed [20,22,34,69,70].

Field observations corroborate Quaternary tectonic activity. Tilted terrace deposits (up to 10° WNW dip), extensional fault networks affecting terrace conglomerates, and normal faults displacing second- and third-order terraces have been mapped in several sites [71]. Localized compressional features within terrace gravels further indicate transient stress changes in an overall extensional regime.

In summary, the Calore River Valley exemplifies the tectonic overprinting of active extension on thrust-related deformation in the Southern Apennines. Its stratigraphic and structural setting, combined with historical and instrumental seismicity, points to a region of significant active tectonic deformation, where near-surface geophysical methods such as GPR can provide new insights into exposed active faults variously related to hidden seismogenic structures.

2. Materials and Methods

Ground Penetrating Radar (GPR) has proven to be a particularly versatile tool for shallow subsurface imaging (on the order of tens of meters in depth), suitable for a wide range of applications, from environmental studies to structural and geological investigations. GPR sounds the ground using high-frequency (typically ranging from 30 to 1000 MHz) electromagnetic pulses generated through an antenna. Pulses propagate through the subsurface and are partially reflected back when they encounter materials with different dielectric properties. Travel time and amplitude of these reflected signals are recorded and used to realize a cross-section of the subsurface. Dielectric permittivity of the subsurface materials primarily governs the radar wave propagation velocity, influencing both the penetration depth and the reflectivity of the encountered interfaces [6,72–76]. Significant dielectric contrasts may result from variations in material composition, water content, porosity, and the presence of fractures or voids. For these reasons, the method is expected to highlight the shallow subsurface lithologic contrasts caused by faults in recent deposits, thus characterizing their current tectonic activity.

In this study, the GPR survey was carried out using a ***COBRA Plug-in SE-70*** system manufactured by Radarteam (Boden, Sweden) (www.radarteam.se). The system was equipped with a monostatic antenna featuring a central frequency of 80 MHz and an effective bandwidth of 120 MHz, covering the frequency range from 20 MHz to 140 MHz. This frequency configuration ensures a suitable trade-off between vertical resolution and penetration depth, allowing signal propagation and target detection down to approximately 50 m under the specific soil and sediment properties of the study area. The system recorded data at a sampling rate of 32,000 samples per second, providing a signal-to-noise ratio of 45 dB [7]. The acquisition was conducted by manually towing the antenna along predefined survey lines at constant speed.

The raw GPR data underwent a multi-stage processing workflow aimed at enhancing signal quality, suppressing noise, and enabling precise subsurface interpretation, as summarized in Figure 3 and described in the following.

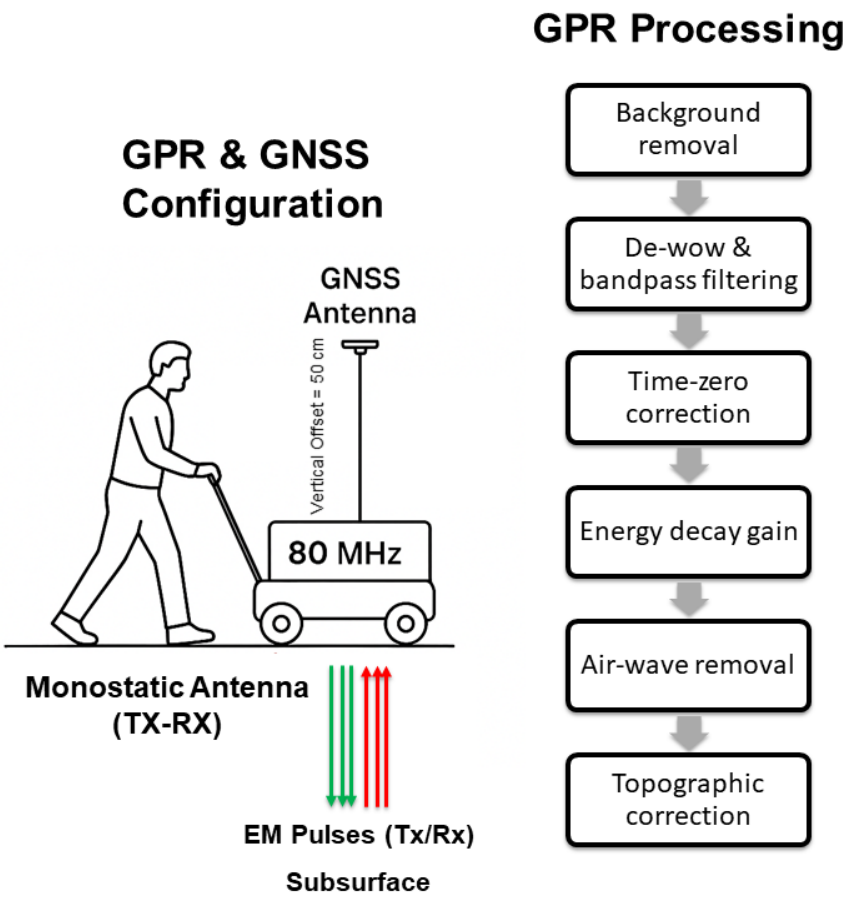


Figure 3. Configuration of the Ground Penetrating Radar (GPR) survey coupled with a GNSS system (**left**) and main steps of the GPR data processing workflow (**right**). The scheme illustrates the monostatic antenna setup with electromagnetic wave transmission and reception, GNSS antenna positioning with vertical offset, and the sequence of processing steps applied to the GPR raw data.

- The first stage involved the removal of temporally incoherent signals using a background-removal ***filter***, which eliminated static or environmental noise unrelated to genuine subsurface reflections. This was followed by the application of ***de-wow filters*** to correct low-frequency drift and ***bandpass filters*** to isolate the frequency range of interest [77–79]. In particular, a band-pass frequency filter with cutoff frequencies of 35 MHz (lower) and 130 MHz (upper) and a filter order of 40 was applied to enhance signal clarity and preserve the most relevant subsurface reflections.
- Then, a ***time-zero correction*** was performed to eliminate the initial portion of the radar trace that corresponds to internal system responses rather than subsurface reflections. This correction is essential, as failing to remove the system's "dead time" would lead to erroneous depth calculations and incorrect positioning of reflectors [80,81].
- Subsequently, ***energy decay gain*** was applied to balance the progressive attenuation of the radar signal with depth. This method calculates the average amplitude decay curve for all traces in a radar profile and then applies a gain function that compensates for this attenuation. The result is a more uniform amplitude distribution across the depth axis, improving the visibility of deeper reflectors and facilitating the interpretation of the entire profile [82,83].
- The next step of the process addressed the ***removal of air-wave reflections***, which are above-ground signals caused by electromagnetic waves reflecting off surrounding objects such as trees, buildings, vehicles, or personnel. These reflections, although not

originating from the subsurface, can contaminate the data and were attenuated using specific filtering techniques especially effective against distant air-wave signals [84,85].

- The ***spatial positioning*** of the radar data was then achieved using high-precision GNSS receivers connected in RTK (Real-Time Kinematic) mode to the INGV-RING Network [68] (https://doi.org/10.13127/ring; accessed on 8 February 2024), using the VITU station as a reference (VITU00ITA—Vitulano (Bn), Campania, Italy). The integration of GNSS positioning ensured centimeter-level accuracy in planimetry. A vertical offset correction of 50 cm was also applied to account for the physical distance between the GNSS antenna's phase center and the GPR dipole center, allowing the radar reflections to be projected onto the true ground surface with correct elevation [86,87].
- Finally, to further improve spatial accuracy, a ***topographic correction*** was implemented by integrating the GNSS-derived elevation data with the radar profiles. This correction repositions each radar trace based on the local topography, allowing the radargrams to reflect the true geometry of the terrain and ensuring that all subsurface features refer to the actual surface morphology [88,89].
- Migration was not applied, as the main goal was to preserve the true travel- time geometry and reflector continuity for correlation with field observations. Preliminary tests using Stolt migration did not significantly improve reflector focusing and slightly reduced the interpretability of deeper reflections.

Data were processed and analyzed using the software platforms Prism-2 (https://www.radsys.lv) and Geolitix (https://www.geolitix.com). Prism-2 provided tools for acquisition, monitoring, gain control and profile editing, while Geolitix was used for the detailed interpretation of 2D radargrams and reconstruction of subsurface features. These platforms allowed for the identification of key structures such as lithological boundaries, sedimentary discontinuities, and potential tectonic features including fault planes and fracture zones [90,91].

The combination of broadband GPR system, high-precision GNSS positioning, and advanced signal processing techniques enabled detailed imaging of the shallow subsurface and provided valuable insights into the stratigraphic and structural setting of the investigated area demonstrating, as described in the following sections, the potential of this method in the considered geological conditions [6,7].

Quantitative analyses such as CMP velocity modeling or coherence attribute extraction were not performed, as the acquisition geometry and field conditions limited multi-offset recording. Instead, qualitative amplitude and continuity analyses were carried out, cross-validated with field structural and stratigraphic observations.

GPR Data Acquisition: Survey Areas and Technical Details

The primary objective of this study was the systematic acquisition of Ground Penetrating Radar (GPR) profiles to assess the efficacy of this geophysical method in detecting and characterizing potentially active tectonic structures associated with the Calore River Fault System. Two distinct survey areas were selected based on preliminary field surveys and on detailed analyses of existing remote sensing and geospatial datasets, which identified zones with the highest structural and stratigraphic potential.

A total of ten GPR profiles were acquired across the study areas, along a total of 1899 m tracks. Acquisition parameters, including antenna frequency and time window, were meticulously chosen to the anticipated subsurface target depth to optimize both signal penetration and survey resolution. This approach ensured that the GPR profiles could effectively image the specific geological features of interest, as a detailed stratigraphy and meso-structural feature (i.e., fractures and faults). Where feasible, individual survey lines were recorded using multiple antenna frequencies, a technique that facilitated multi-scale

subsurface imaging and enabled the crucial discrimination between stratigraphic horizons and subtle structural discontinuities [7].

The locations of selected and hereinafter commented profiles are presented in Figure 4, with a summary of survey lines, acquisition parameters, and corresponding study areas reported in Table 1.

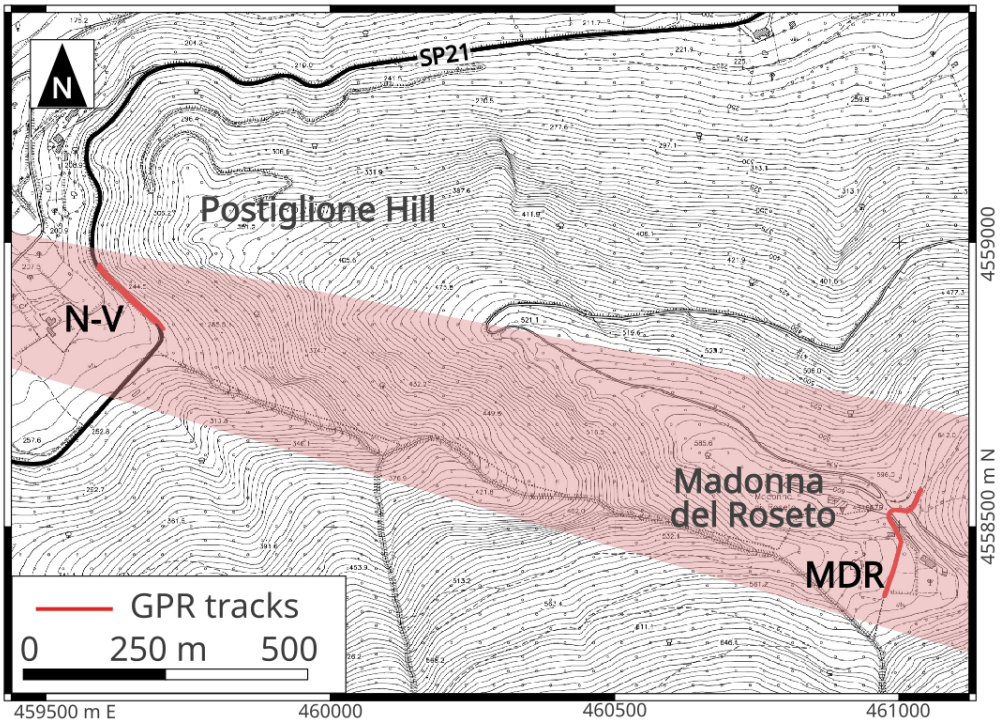


Figure 4. Map showing the GPR survey layout. The red lines indicate the discussed GPR profiles (Table 1), grouped into the sectors N–V (main Postiglione Fault outcrop along the SP21 street), and MDR (Madonna del Roseto church, Solopaca town). The pink-shaded area represents the Postiglione Fault region of influence. The base map is derived from a 1:5000 digital topographic map (Carta Tecnica Regionale, Regione Campania, 2005).

Table 1. Summary of discussed GPR profiles.

Profile Name	Investigated Depth (m)	Frequency (MHz)	Profile Length (m)
MDR1	5	120	259
MDR2	15	80	236
MDR3	25	60	232
MDR4	35	40	234
N1	15	80	188
N2	25	60	187
N3	25	60	165
N4	15	80	158
V1	25	60	155
V2	50	30	85

GPR data acquisition was systematically performed across the study area. In detail, two distinct sites were deeply sounded and commented in this paper, due to key geological and geomorphological features useful to constrain the definition of the shallow evidence of

recent tectonic activities in the Calore River Valley. Madonna del Roseto area is a hendoreic basin, WNW–ESE elongated, hosted above a Mesozoic carbonate substratum and topped by a low-tickness eluvial–colluvial sedimentary succession (late Pleistocene–Holocene) (Figures 4 and 5; [62]). The Postiglione hill is the western termination of the Taburno–Camposauro Mts. carbonate massif, made up of Meso-Cenozoic successions derived by Apennine Carbonate Platform. Postiglione site of survey is located at the foothill sector, along an artificial cut along the SP21 road. This outcrop was described by different authors during the last decades as it beautifully shows the Postiglione Fault main fault- core (Figures 4 and 6; [34,35]).

➢ Madonna del Roseto area:

In the Madonna del Roseto area (Figure 4), four GPR profiles (***MDR1–MDR4)***, were acquired along the same profile, indicated in Figure 4 by the red line labeled MDR, to investigate the subsurface of the small WNW–ESE trending valley described above. These profiles, ranging from 232 to 259 m in length, were oriented NNE–SSW, in an area with elevations between 596 and 609 m a.s.l. A multi-frequency approach was adopted to achieve a multi-scale characterization, with each survey employing a different frequency and corresponding penetration depth:

1. 120 MHz: Provided high-resolution imaging of the shallow subsurface, with an investigation depth of approximately 5 m (MDR1 profile).
2. 80 MHz: Allowed for a deeper investigation down to approximately 15 m (MDR2 profile).
3. 60 MHz: Extended the depth of investigation to about 25 m (MDR3 profile).
4. 40 MHz: Achieved the maximum penetration depth of approximately 35 m, allowing for the detection of deeper geological features (MDR4 profile).

For time-to-depth conversion, a constant propagation velocity of 0.1 m/ns (corresponding to a dielectric constant of 9) was adopted. The velocity value was derived from literature data [34,35,43] and verified through hyperbola fitting of clear point reflectors identified in the radar profiles. This approach was critical for differentiating shallow stratigraphic features from deeper structural discontinuities potentially associated with fault activity.

➢ Postiglione area:

A set of four profiles (***N1–N4***) was acquired along the Frasso–Solopaca provincial road (SP21, Figure 4) on the same survey line, indicated in Figure 4 by the red line labeled N–V, where the local elevation is about 250 m a.s.l. The surveyed profiles, measuring between 158 and 188 m in length, were recorded using the multiple-frequency approach. The use of both an 80 MHz and a 60 MHz antenna retrieved the most accurate view of the subsurface, with estimated penetration depths of approximately 15 and 25 m, respectively. This approach aimed to achieve both moderate resolution and sufficient depth to characterize potential subsurface structures in this location.

Two additional profiles, ***V1*** and ***V2***, were acquired along artificial cuts of the SP21 road, abovementioned as the Postiglione Fault main fault- core outcrop (Figures 2 and 4). These profiles were collected parallel to the outcrop using a horizontal acquisition geometry, with the GPR antenna illuminating the vertical cut. Although logistically more complex, this configuration provided valuable geological and structural constraints for interpreting the data in relation to visible surface features, complementing the classical geometrical approach adopted for the N profiles. The V1 and V2 profiles were acquired using different antenna frequencies to maximize the investigative depth range:

1. Profile V1: a 155 m-long profile acquired with a 60 MHz antenna, enabling an investigation depth of approximately 25 m.
2. Profile V2: an 85 m-long profile acquired with a low-frequency 30 MHz antenna, which allowed for a significantly greater penetration depth of up to 50 m.

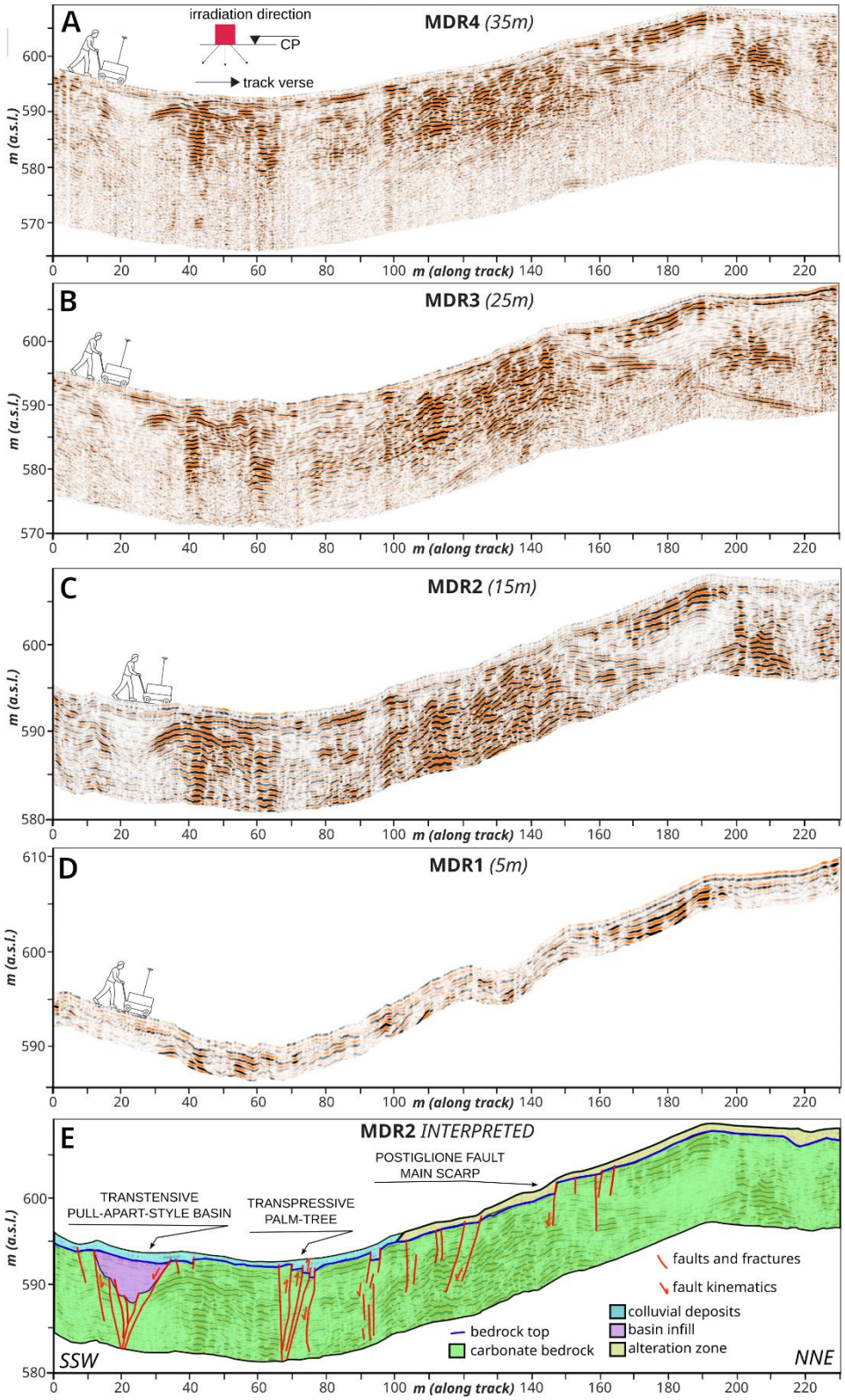


Figure 5. Processed GPR radargrams (see Figure 4 for location and Table 1 for details): (**A**) MDR4 (~35 m penetration). (**B**) MDR3 (~25 m penetration). (**C**) MDR2 (~15 m penetration). (**D**) MDR1 (~5 m penetration). Radargrams show different reflection patterns, including semi-transparent reflections, plane-parallel horizons, and deformed reflections. (**E**) Geological and structural interpretation of MDR2 radargram: colluvial deposits (light brown), fractured carbonate bedrock and cataclasites (green), and steeply dipping normal faults (red lines), including the main SSE-dipping fault plane.

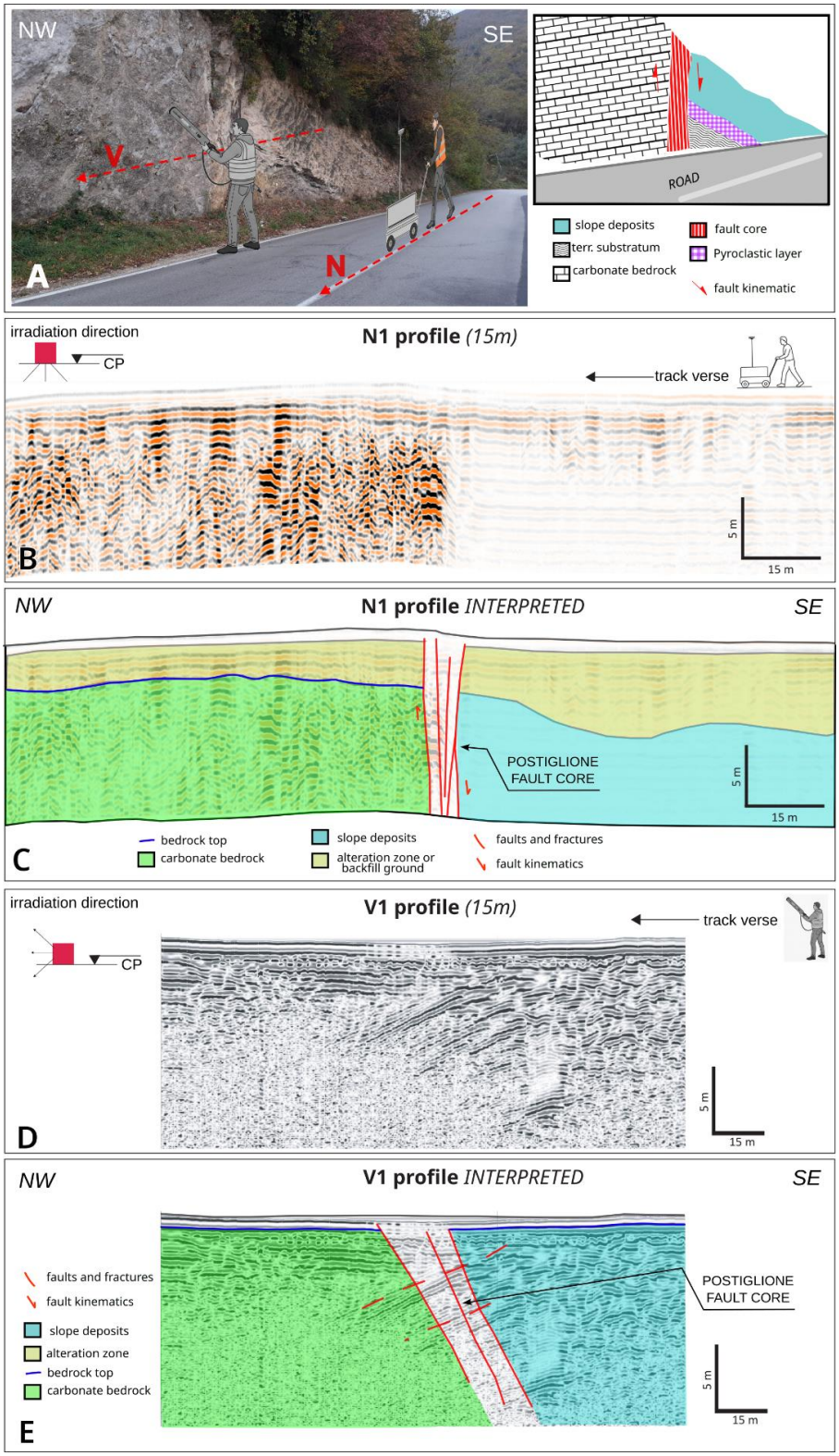


Figure 6. (**A**) Field photo of the Postiglione Fault outcrop along the SP21, showing the trace of GPR profiles N1 and V1 and the acquisition geometries; in the upper right inset, a schematic structural sketch is shown. (**B**) Processed radargram of profile N1 (188 m, SSE–NNW, 80 MHz, ~15 m penetration), acquired with radiation towards the ground, showing semi-transparent zones, plane-parallel horizons. (**C**) Structural interpretation of N1. (**D**) Processed radargram of profile V1 (155 m, SSW–NNE, 60 MHz, ~25 m penetration), acquired with horizontal irradiation toward the scarp, displaying chaotic reflections and reflector truncations. (**E**) Structural interpretation of V1.

3. Results

The Ground Penetrating Radar (GPR) survey yielded high-resolution images of the shallow subsurface in specific sites of the Calore River Valley area, enabling the identification of active fault-related structures and associated deformation volumes. Across the different survey sites, radargrams consistently revealed steeply dipping discontinuities, reflector truncations, and localized scattering, which we interpret as indicators of fault planes, damage zones, and eluvial–colluvial deposits.

➢ Madonna del Roseto area

The multiple frequency approach allowed the acquisition of a wide range of details across a subsurface volume up to 35 m of depth. All radargrams were interpreted using a line-drawing procedure that enabled the retrieving of the deepest possible evidence of the stratigraphic and structural setting of the surveyed volume. Among the four profiles, the most representative is MDR2 (236 m, SSE–NNW, 80 MHz, ~15 m penetration); its detailed structural interpretation is summarized in Figure 5E.

The interpreted radargram (Figure 5E) reveals two main domains: (i) the upper part, characterized by semi-transparent to parallel reflections associated with unconsolidated eluvial–colluvial deposits; and (ii) the deeper part of the section, where discontinuous and chaotic reflections mark fractured carbonate bedrock and cataclastic horizons (solid blue line in Figure 5E). The depth of useful data retrieving can be approximately identified at 25 m. Sections show a clear eluvial–colluvial depositional succession above an intensely fractured and faulted carbonatic substratum. The carbonate bedrock shows a steeply dipping swarm of reflectors (at about 150 m along the profile) that truncate reflectors corresponding to carbonate substratum strata; these sub-vertical reflectors can be interpreted as the main scarp of the Postiglione Fault.

Evidence of transpressive and transtensive related structures were also retrieved: (i) a transtensive pull-apart-like basin can be retrieved just at the SSW termination of the section (at about 20 m along track); this narrow basin shows an infill of fine grained deposits, compatible with an ephemeral lacustrine environment; (ii) a transpressive push-up "palm-tree" structure can be identified at about 70 m SSW (Figure 5C,E). Overall, the Madonna del Roseto basin has been developing above the fault core of the Postiglione Fault, fault and fracture systems were retrieved across a wide portion of the MDR sections, defining an extension up to 70 m-wide (Figure 5E).

The wedge-shaped geometry of the deposits and the abrupt reflector terminations are consistent with the development of a small fault-bounded depocenter, which can be interpreted as the product of repeated Holocene surface faulting events, consistent with dip- and strike-slip kinematics along a complex arrangement of fault splays.

➢ Postiglione area

In the Postiglione foothill site (Figure 4), radar profiles were acquired parallel to the main fault scarp, with both vertical and horizontal irradiation geometries, as detailed in the previous section, in order to test the effectiveness of the method in constraining the setting of the carbonate bedrock and the deformation zone related to the Postiglione Fault (Figures 4 and 6).

Figure 6A shows a field view of the SP21 road outcrop, an artificial cut showing the main deformation zone associated with a sub-vertical fault with evidence of both dip- and strike-slip clues:

- slickenside lineations clueing pure dip-slip kinematic, associated with geological evidence, involvement of slope deposits and embedded pyroclastics in faulting;
- remarkable hooking of slope deposits pseudo-strata and pyroclastics, compatible with a strike-slip component along the Postiglione Fault.

The NW hanging wall consists of Jurassic–Cretaceous calcarenites belonging to tectonic units of the Apennine Carbonate Platform, the SE footwall shows a succession made up of a terrigenous substratum (late Miocene) covered by a carbonate breccia in sandy matrix, i.e., the slope deposits of the Postiglione hill. This deposit embeds, in the lower portion, a reworked pyroclastic layer made up of glass, pumice and sanidine crystals, with an $^{40}Ar/^{39}Ar$ age of 45 ± 5 ka [34], the entire footwall succession has been recently dated younger than 9 ka [35]. This structure is considered the most recent evidence of faulting in the study area and one of the latest of the whole Sannio–Matese District. The survey lines and the adopted acquisition geometries are also reported in Figure 6A.

Approaching the line drawing of the acquired radargrams, a schematic representation of the main reflectors and features visible in the radar profile, highlighting structural or stratigraphic elements without showing the full raw amplitude data, we discuss a synthesis of main stratigraphic and structural features of the sensed volume is discussed. The Profile N1 (188 m, SSE–NNW, 80 MHz, ~15 m penetration) (Figure 6B,C) crosses the investigated fault zone at its foothill outcrop. The processed radargram (Figure 6B) shows plane-parallel horizons and semi-transparent zones disrupted by a 7–8 m wide corridor of chaotic reflections and diffraction hyperbolae between 70–80 m along the transect. The interpretation (Figure 6C) highlights the presence of a high-angle S-dipping fault zone affecting the carbonate substratum, accompanied by an intensely fractured damage zone and subsidiary fractures. This volume includes the key features highlighted by V1 and can be reliably considered as the evidence of the Postiglione Fault core. The evanescence of the SE-half section can be due to the presence of loose deposits, locally reworked during the roadbed build (Figure 6C). The V1 profile (155 m, SSW–NNE, 60 MHz, ~25 m penetration) was acquired parallel to the outcrop using a horizontal acquisition geometry (Figure 6D,E) and was conceived to complement the N dataset (see details in previous section). The processed radargram (Figure 6D) shows chaotic reflections and reflector truncations cutting through sub-horizontal horizons. The interpretation (Figure 6E) clearly identifies, at the NW termination, Jurassic–Cretaceous calcarenites belonging to tectonic units of the Apennine Carbonate Platform, which represent the hanging wall of the abovementioned Postiglione Fault. The SE part of the section can be interpreted as a carbonate breccia in a sandy matrix unit, locally arranged as slope deposits of the Postiglione hill. The two parts are in contact along a 7–10 m wide low-coherence zone, interpreted as a set of fault splays of the Postiglione Fault core. The low coherence depends on the presence of a silty–sandy cataclasite at the core of the fault (Figure 6E).

Overall, GPR profiles acquired in both Postiglione and Madonna del Roseto areas are able to detect consistent evidence of active faulting involving late Pleistocene–Holocene up to Recent units of the Calore River Valley and slope depositional units of surrounding carbonate mountains and hills. The profiles reveal steeply dipping normal faults, fractured damage zones, and fault-bounded depocenters infilled by eluvial–colluvial deposits (MDR profiles). These features are coherent with the presence of a fault zone reliably corresponding to the Postiglione Fault (Figure 4). The retrieved features clue an intense activity of the fault system during the late Quaternary and lasting to the Recent age.

The complementary acquisition geometries, vertical and horizontal irradiation, toward the ground and toward the outcrop, and the use of multiple antenna frequencies allowed for an integrated imaging of both shallow stratigraphy and deeper structural evidence. The recognition of stratigraphic offsets, wedge-shaped deposits, and deformation zones provides strong evidence for interpreting the Postiglione Fault as an active tectonic system that exerted a primary control on the recent morphotectonic evolution of the area. We hereby name this as the Postiglione Fault System. These results form the basis for the following Discussion, where the structural evidence imaged by GPR is compared with geological

and geomorphological observations, in order to assess the role of GPR in increasing the definition of the seismotectonic framework of the Sannio–Matese Seismogenic District.

4. Discussion

The application of low-frequency GPR in selected sites of the Calore River Valley (Figure 2) has provided new insights into the shallow structural framework of one of the most seismically active portions of the Southern Apennines. The GPR profiles acquired across the southern sector of the Calore River Valley revealed high-amplitude discontinuities, reflector terminations, and zones of signal scattering that we interpret as indicators of recent and active faulting and associated damage zones. The results are coherent with previous field-based mapping [34,35,62], yet they extend the resolution to subsurface portions where fault traces lack clear surface expression. This is a strong and valuable advance as the adopted approach allowed the retrieving of information with a remote–proximal sensing approach, low cost and fast execution, contrasting with classical direct tranching and sounding typical of the paleoseismological approach.

A key outcome of this work is the capability to identify multiple steeply dipping normal faults, mainly oriented E–W to WNW–ESE, which accommodate an overall extensional deformation along the western flank of Mt. Camposauro, southern bound of the Calore River Valley. GPR data highlight the presence of a complex geometry fault system characterized by sub-vertical fault planes, significant sub-sets of shear structures and sedimentary features, clueing a tectonic history lasting since the late Pleistocene to an age younger than 9 ka. This fault system, here named Postiglione Fault System (PFS), with morphotectonic evidence along the Mt. Camposauro (Figure 2), was barely described by authors in recent decades, probably depending on the very low and sparse surface evidence of its geometries and tectonostratigraphic signature. Our study underlines that the PFS has a greater significance in the recent tectonic evolution of the study region, with respect to the previous beliefs. Such findings support the interpretation of a long-lived, structurally controlled landscape evolution, with repeated phases of surface faulting and basin formation during the late Pleistocene–Recent age.

The GPR detection of eluvial–colluvial deposits and buried basin infills provides further evidence of fault activity. Madonna del Roseto profiles (MDR1–MDR4) clearly delineated small fault-driven depocenters, which can be interpreted as the morphological and stratigraphic response to coseismic deformation. These features are consistent with previously reported observations of terrace tilting and faulted conglomerates in this area [71]. The integration of vertical and horizontal acquisition geometries (profiles N1 and V1) proved especially useful to distinguish between lithological boundaries and tectonic structures, confirming the capability of GPR to discriminate between fault-related reflectors even in heterogeneous sedimentary successions, preventing the use of expensive and invasive classical techniques, typical in paleoseismology studies (trenching, excavations, direct stratigraphic techniques).

From a methodological point of view, the adoption of a broadband low-frequency antenna with a central frequency of 80 MHz, operated in multiple frequency configurations, enabled imaging depths down to 30–35 m while retaining adequate vertical resolution, up to 40 cm, to resolve fault-related features and stratigraphies. This option is particularly valuable in defining tectonic settings where faults are expressed as steep, narrow zones of fracturing rather than broad stratigraphic offsets. Moreover, the integration with high-precision GNSS positioning and topographic correction has been proved essential to achieve a geometrically consistent interpretation, especially where profiles were collected along irregular ground surfaces and/or remote regions.

Although forward modeling or synthetic waveform analysis was not performed, our radar interpretations were validated through direct geological and stratigraphic observations at outcrop scale, ensuring a consistent correlation between radar responses and observed fault geometries. Given the heterogeneity of the surveyed deposits and the complex acquisition geometries, realistic forward modeling would require numerous simplifying assumptions that could reduce representativeness of the actual field conditions.

Structural measurements collected in the field were used qualitatively to support the kinematic interpretation of the fault system. However, their spatial distribution and the limited exposure of fresh fault planes prevented construction of statistically robust fault-slip rosettes or fault-plane solutions. Targeted structural surveys and kinematic sampling (to obtain measurable slip vector populations and compute fault-plane solutions) are therefore planned for future work to quantitatively corroborate the inferred kinematics.

When compared with other geophysical approaches, such as seismic reflection or electrical resistivity tomography, low-frequency GPR emerges as a cost-effective and non-invasive tool particularly suited to reconnaissance-scale investigations. Although penetration is limited in clay-rich or highly conductive deposits, the lithological conditions of the Calore River Valley and its surroundings, characterized by gravels, sands, and fractured carbonates, proved favorable for radar wave propagation. The success of this application suggests that similar surveys could be extended to other similar regions where the surface evidence of faulting is subtle or absent.

Overall, the GPR dataset corroborates the hypothesis that the Calore Valley area has been affected by late Pleistocene to recent age tectonic activity, supporting the key role played by the PFS. These results provide independent support for seismotectonic models that associate destructive historical earthquakes, such as the 1688 Sannio event (Mw 7.06), with fault systems in this sector [31,34,35].

5. Conclusions

This study demonstrates the effectiveness of Ground Penetrating Radar (GPR) for detecting and characterizing active fault structures in active tectonic areas. It also highlights how this technique requires proper location and orientation of the acquisition traces, guided by geological expertise. This integrated approach multiplies the effectiveness of GPR in active tectonics and young deposits environments. As a target zone, we selected the Calore River Valley, one of the most promising areas across the Southern Apennines.

At Madonna del Roseto Area, GPR profiles imaged a steep normal fault system truncating the carbonate bedrock and bounding a wedge-shaped depocenter filled with eluvial–colluvial deposits. The reflector truncations and stratigraphic architecture provide robust evidence of repeated late Pleistocene to Recent surface faulting.

At Postiglione hill, N-V profiles detailed the geometry of the damage zone associated with the Postiglione Fault System (PFS), characterized by a sub-vertical SSE-dipping main fault plane, chaotic reflection zones, and splays indicating intense fracturing and distributed deformation across the fault zone.

The results are summarized in the conceptual model shown in Figure 7, which integrates GPR evidence, structural interpretations, and geomorphological observations, along with literature. GPR results allow a highly detailed view of the actual geometry and evidence of kinematic behavior of the PFS, which appears as a system with a complex slipping history. The evidence of both dip-slip and strike-slip kinematics gives a novel and robust view of this fault zone. The model of Figure 7 illustrates the architecture of the PFS as a segmented, steeply fault splay controlling fault-bounded depocenters and damage zones involving the carbonate substratum of the Taburno–Camposauro Mts and associated slope deposits.

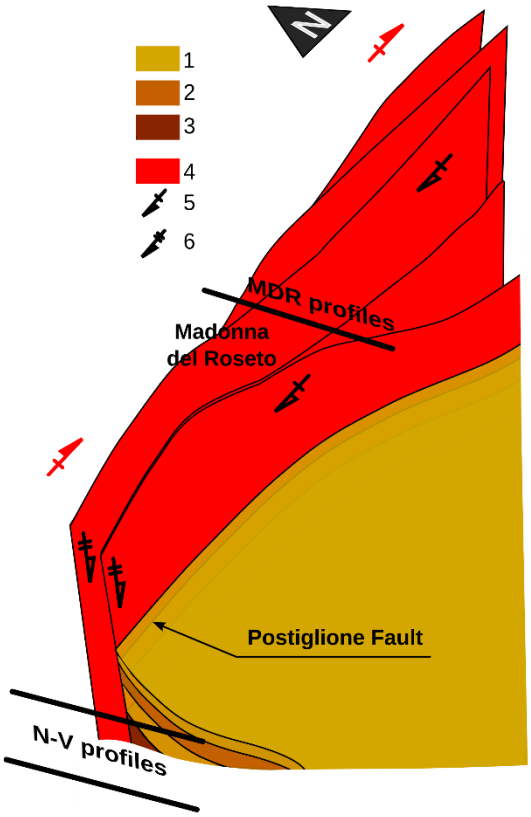


Figure 7. Structural interpretation of the Postiglione Fault System (PFS). 1. Late Pleistocene–Holocene colluvial and slope deposits; 2. Pyroclastic layer (45–9 ka); 3. Pre-Quaternary terrigenous substratum (late Miocene); 4. Fault splays of the Postiglione Fault zone; 5. Strike-slip kinematics; 6. Dip-slip kinematics. N-V: near-vertical. The location of the proposed model roughly corresponds to the pink region of Figure 4.

In this geologically complex region, where seismogenic sources remain debated but historical seismicity is significant (e.g., the 1688 Mw 7.06 Sannio earthquake), we have identified several shallow discontinuities that may correspond to faults linked to one of the proposed sources. The PFS, in particular, can be regarded as a shallow, antithetical system to the known seismogenic Calore River Fault System (CRFS, [34]), providing complementary evidence of active tectonics in the area. Future work will aim to clarify the relationship between these shallow structures and the deeper seismogenic source.

The retrieved evidence of recent activity supports a novel role for an underestimated fault system: the Postiglione Fault System acts as the shallow expression of the CRFS, with both systems playing a key role in the active tectonics and morphotectonic evolution of the Sannio–Matese region. The presence of both dip- and strike- –slip kinematics supports the identification of right-lateral and left-lateral splays along the PFS main fault, allowing the contemporary development of transtensive and transpressive features, and more generally the occurrence of strike-slip kinematics in an extensional tectonic regime. This includes the:

- ➢ pull-apart-style basin and the palm-tree push-up range depicted by MDR survey (Figure 5);
- ➢ unusual strata hooks reported at the Postiglione downhill outcrop.

Such evidence is often barely visible at surface, where the dip-slip normal kinematics can obscure the meso-structural evidence of this complex tectonic behavior. This framework strengthens the interpretation of the PFS as an active fault system, younger than 9 k years, identifiable in a thin, highly deformed fault zone (7–10 m thick) at the downhill site with cataclasite and strata hooking (Figure 6A), which widens to at least 70 m at Madonna

del Roseto, where buried mesostructures typical of local transtension and transpression are preserved.

Beyond the specific case study, the successful application of low-frequency GPR highlights the methodological potential of this technique for investigating active faults in a carbonate substratum and overlying fine-to-coarse-grained sedimentary units. By refining the shallow structural framework where surface evidence is scarce, GPR contributes to the improvement of seismotectonic models and enhances seismic hazard assessment in one of the most tectonically active regions of the Mediterranean.

Author Contributions: Conceptualization, N.A.F. and B.M.; methodology, N.A.F. and B.M.; software, N.A.F. and B.M.; validation, N.A.F., G.M., A.M., R.M., N.G., D.D.B., D.C., A.V. and B.M.; investigation, N.A.F. and B.M.; data curation, N.A.F. and B.M.; writing—original draft preparation, N.A.F., G.M., A.M., R.M., N.G., D.D.B., D.C., A.V. and B.M.; writing—review and editing, N.A.F., G.M., A.M., R.M., N.G., D.D.B., D.C., A.V. and B.M.; visualization, ALL. All authors have read and agreed to the published version of the manuscript.

Funding: This research received no external funding.

Data Availability Statement: The original contributions presented in this study are included in the article. Further inquiries can be directed to the corresponding author.

Conflicts of Interest: The authors declare no conflicts of interest.

References

1. Knight, R. Ground Penetrating Radar for Environmental Applications. *Annu. Rev. Earth Planet. Sci.* **2001**, *29*, 229–255. [CrossRef]
2. Hubbard, S.; Chen, J.; Williams, K.; Peterson, J.; Rubin, Y. Environmental and Agricultural Applications of GPR. In Proceedings of the 3rd International Workshop on Advanced Ground Penetrating Radar, Delft, The Netherlands, 2–3 May 2005.
3. Wai-Lok Lai, W.; Dérobert, X.; Annan, P. A Review of Ground Penetrating Radar Application in Civil Engineering: A 30-Year Journey from Locating and Testing to Imaging and Diagnosis. *NDT E Int.* **2018**, *96*, 58–78. [CrossRef]
4. Lombardi, F.; Podd, F.; Solla, M. From Its Core to the Niche: Insights from GPR Applications. *Remote Sens.* **2022**, *14*, 3033. [CrossRef]
5. Ercoli, M.; Cirillo, D.; Pauselli, C.; Jol, H.M.; Brozzetti, F. Ground-Penetrating Radar Signature of Quaternary Faulting: A Study from the Mt. Pollino Region, Southern Apennines, Italy. *Solid Earth* **2021**, *12*, 2573–2596. [CrossRef]
6. Davis, J.L.; Annan, A.P. Ground-Penetrating Radar for High-Resolution Mapping of Soil and Rock Stratigraphy. *Geophys. Prospect.* **1989**, *37*, 531–551. [CrossRef]
7. Famiglietti, N.A.; Miele, P.; Massa, B.; Memmolo, A.; Moschillo, R.; Zarrilli, L.; Vicari, A. Ground Penetrating Radar (GPR) Investigations in Urban Areas Affected by Gravity-Driven Deformations. *Geosciences* **2024**, *14*, 222. [CrossRef]
8. Grasmueck, M.; Eberli, G.P. 3D Gpr Stratal Slicing of Sedimentary Structures. In Proceedings of the 2025 13th International Workshop on Advanced Ground Penetrating Radar (IWAGPR), Thessaloniki, Greece, 2–4 July 2025; pp. 1–5.
9. Fountoulis, I.; Vassilakis, E.; Mavroulis, S.; Alexopoulos, J.; Dilalos, S.; Erkeki, A. Synergy of Tectonic Geomorphology, Applied Geophysics and Remote Sensing Techniques Reveals New Data for Active Extensional Tectonism in NW Peloponnese (Greece). *Geomorphology* **2015**, *237*, 52–64. [CrossRef]
10. Jamšek Rupnik, P.; Atanackov, J.; Horn, B.; Mušič, B.; Zajc, M.; Grützner, C.; Ustaszewski, K.; Tsukamoto, S.; Novak, M.; Milanič, B.; et al. Revealing Subtle Active Tectonic Deformation: Integrating Lidar, Photogrammetry, Field Mapping, and Geophysical Surveys to Assess the Late Quaternary Activity of the Sava Fault (Southern Alps, Slovenia). *Remote Sens.* **2024**, *16*, 1490. [CrossRef]
11. Cheloni, D.; D'Agostino, N.; Scognamiglio, L.; Tinti, E.; Bignami, C.; Avallone, A.; Giuliani, R.; Calcaterra, S.; Gambino, P.; Mattone, M. Heterogeneous Behavior of the Campotosto Normal Fault (Central Italy) Imaged by InSAR GPS and Strong-Motion Data: Insights from the 18 January 2017 Events. *Remote Sens.* **2019**, *11*, 1482. [CrossRef]
12. DISS Working Group. Database of Individual Seismogenic Sources (DISS). 2025. Available online: http://diss.ingv.it/data/ (accessed on 20 August 2025).
13. Fracassi, U.; Milano, G. A Soft Linkage between Major Seismogenic Fault Systems in the Central-Southern Apennines (Italy): Evidence from Low-Magnitude Seismicity. *Tectonophysics* **2014**, *636*, 18–31. [CrossRef]
14. Milano, G.; Di Giovambattista, R.; Ventura, G. Seismic Activity in the Transition Zone between Southern and Central Apennines (Italy): Evidences of Longitudinal Extension inside the Ortona–Roccamonfina Tectonic Line. *Tectonophysics* **2008**, *457*, 102–110. [CrossRef]

15. Ferranti, L.; Milano, G.; Burrato, P.; Palano, M.; Cannavò, F. The Seismogenic Structure of the 2013–2014 Matese Seismic Sequence, Southern Italy: Implication for the Geometry of the Apennines Active Extensional Belt. *Geophys. J. Int.* **2015**, *201*, 823–837. [CrossRef]
16. Rovida, A.; Locati, M.; Camassi, R.; Lolli, B.; Gasperini, P.; Antonucci, A. Italian Parametric Earthquake Catalogue CPTI15, Version 4.0. *Bull. Earthq. Eng.* **2021**, *4*, 2953–2984.
17. CPTI15-DBMI15 2022. Available online: https://emidius.mi.ingv.it/CPTI15-DBMI15/query_place/ (accessed on 18 January 2025).
18. Montone, P.; Amato, A.; Pondrelli, S. Active Stress Map of Italy. *J. Geophys. Res. Solid Earth* **1999**, *104*, 25595–25610. [CrossRef]
19. Montone, P.; Mariucci, M.T.; Pondrelli, S.; Amato, A. An Improved Stress Map for Italy and Surrounding Regions (Central Mediterranean). *J. Geophys. Res. (Solid Earth)* **2004**, *109*, B10410. [CrossRef]
20. Montone, P.; Mariucci, M.T.; Pierdominici, S. The Italian Present-Day Stress Map. *Geophys. J. Int.* **2012**, *189*, 705–716. [CrossRef]
21. Pierdominici, S.; Mariucci, M.T.; Montone, P. A Study to Constrain the Geometry of an Active Fault in Southern Italy through Borehole Breakouts and Downhole Logs. *J. Geodyn.* **2011**, *52*, 279. [CrossRef]
22. De Matteo, A.; Massa, B.; Milano, G.; D'Auria, L. A Transitional Volume beneath the Sannio-Irpinia Border Region (Southern Apennines): Different Tectonic Styles at Different Depths. *Tectonophysics* **2018**, *723*, 14–26. [CrossRef]
23. Westaway, R. Seismic Moment Summation for Historical Earthquakes in Italy: Tectonic Implications. *J. Geophys. Res. Solid Earth* **1992**, *97*, 15437–15464. [CrossRef]
24. D'Agostino, N. Complete Seismic Release of Tectonic Strain and Earthquake Recurrence in the Apennines (Italy). *Geophys. Res. Lett.* **2014**, *41*, 1155–1162. [CrossRef]
25. Rovida, A.; Antonucci, A.; Locati, M. The European Preinstrumental Earthquake Catalogue EPICA, the 1000–1899 Catalogue for the European Seismic Hazard Model 2020. *Earth Syst. Sci. Data* **2022**, *14*, 5213–5231. [CrossRef]
26. Bernard, P.; Zollo, A. The Irpinia (Italy) 1980 Earthquake: Detailed Analysis of a Complex Normal Faulting. *J. Geophys. Res. Solid Earth* **1989**, *94*, 1631–1647. [CrossRef]
27. Boschi, E. *Special Issue on the Meeting "Irpinia Dieci Anni Dopo": Sorrento, November 19–24, 1990*; Istituto Nazionale di Geofisica: Roma, Italy, 1993.
28. Borraccini, F.; Donatis, M.D.; Bucci, D.D.; Mazzoli, S. 3D Model of the Active Extensional Fault System of the High Agri River Valley, Southern Apennines, Italy. *J. Virtual Explor.* **2002**, *6*, 1–6. [CrossRef]
29. Burrato, P.; Valensise, G. Rise and Fall of a Hypothesized Seismic Gap: Source Complexity in the Mw 7.0 16 December 1857 Southern Italy Earthquake. *Bull. Seismol. Soc. Am.* **2008**, *98*, 139–148. [CrossRef]
30. Di Bucci, D.; Corrado, S.; Naso, G. Active Faults at the Boundary between Central and Southern Apennines (Isernia, Italy). *Tectonophysics* **2002**, *359*, 47–63. [CrossRef]
31. Pantosti, D.; Valensise, G.; Pantosti, D.; Valensise, G. La Faglia Sud-Appenninica: Identificazione Oggettiva Di Un Lineamento Sismogenetico Nell'Appennino Meridionale. In Proceedings of the 7th Meeting Gruppo Nazionale di Geofisica della Terra Solida, Rome, Italy, 28–30 November 1988.
32. Gasperini, P.; Bernardini, F.; Valensise, G.; Boschi, E. Defining Seismogenic Sources from Historical Earthquake Felt Reports. *Bull. Seismol. Soc. Am.* **1999**, *89*, 94–110. [CrossRef]
33. Valensise, G.; Pantosti, D. Seismogenic Faulting, Moment Release Patterns and Seismic Hazard along the Central and Southern Apennines and the Calabrian Arc. In *Anatomy of an Orogen: The Apennines and Adjacent Mediterranean Basins*; Vai, G.B., Martini, I.P., Eds.; Springer Netherlands: Dordrecht, The Netherlands, 2001; pp. 495–512; ISBN 978-94-015-9829-3.
34. Di Bucci, D.; Massa, B.; Zuppetta, A. Relay Ramps in Active Normal Fault Zones: A Clue to the Identification of Seismogenic Sources (1688 Sannio Earthquake, Italy). *GSA Bull.* **2006**, *118*, 430–448. [CrossRef]
35. Amato, V.; Ciarcia, S.; Galli, P.; Cicchella, D.; Galderisi, A.; Monaco, L.; Fernandez, G.; Isaia, R.; Nomade, S.; Pereira, A.; et al. Unveiling the Hidden Source of Major Historical Earthquakes: A Multi-Scale, Trans-Disciplinary Approach to the 1456 and 1688 Sannio Earthquakes (Mw 7.0, Southern Italian Apennines). *Quat. Sci. Rev.* **2025**, *356*, 109282. [CrossRef]
36. Calabrò, R.A.; Corrado, S.; Di Bucci, D.; Robustini, P.; Tornaghi, M. Thin-Skinned vs. Thick-Skinned Tectonics in the Matese Massif, Central–Southern Apennines (Italy). *Tectonophysics* **2003**, *377*, 269–297. [CrossRef]
37. Galadini, F. Pleistocene Changes in the Central Apennine Fault Kinematics: A Key to Decipher Active Tectonics in Central Italy. *Tectonics* **1999**, *18*, 877–894. [CrossRef]
38. Galandini, F.; Galli, P. Paleoseismology Related to Deformed Archaeological Remains in the Fucino Plain. Implications for Subrecent Seismicity in Central Italy. *Ann. Geophys.* **1996**, *39*, 925–940. [CrossRef]
39. Pantosti, D.; D'Addezio, G.; Cinti, F.R. Paleoseismicity of the Ovindoli-Pezza Fault, Central Apennines, Italy: A History Including a Large, Previously Unrecorded Earthquake in the Middle Ages (860-1300 A.D.). *J. Geophys. Res.* **1996**, *101*, 5937–5959. [CrossRef]
40. Cinti, F.R.; Cucci, L.; Pantosti, D.; D'Addezio, G.; Meghraoui, M. A Major Seismogenic Fault in a 'Silent Area': The Castrovillari Fault (Southern Apennines, Italy). *Geophys. J. Int.* **1997**, *130*, 595–605. [CrossRef]

41. Michetti, A.M.; Ferreli, L.; Serva, L.; Vittori, E. Geological Evidence for Strong Historical Earthquakes in an "Aseismic" Region: The Pollino Case (Southern Italy). *J. Geodyn.* **1997**, *24*, 67–86. [CrossRef]
42. Mazzoli, S.; Helman, M. Neogene Patterns of Relative Plate Motion for Africa-Europe: Some Implications for Recent Central Mediterranean Tectonics. *Geol. Rundsch.* **1994**, *83*, 464–468. [CrossRef]
43. D'Argenio, B. Carta Geologica Del Gruppo Del Taburno Camposauro, Scala 1:50.000. *Atti Accad. Delle Sci. Fis. Mat. Napoli S. 3a* **1965**, *5*.
44. Pescatore, T.S.; Sgrosso, I.; Torre, M. Lineamenti Di Tettonica e Sedimentazione Nel Miocene Dell'Appennino Campano-Lucano: Memorie Della Società Naturalisti in Napoli. *Mem. Soc. Nat.* **1970**, *78*, 337–408.
45. Mostardini, F.; Merlini, S. Appennino Centro Meridionale: Sezioni Geologiche e Proposta di Modello Strutturale, Agip. 1986. Available online: http://pascal-francis.inist.fr/vibad/index.php?action=getRecordDetail&idt=8170990 (accessed on 18 January 2025).
46. Patacca, E.; Scandone, P. The Geological Map of Sannio and Surrounding Areas by Raimondo Selli (Scale 1:100,000). A Precious Collection of Still Current Data. *Boll. Soc. Geol. Ital.* **2005**, *4*, 17–30.
47. Patacca, E.; Scandone, P. Geology of the Southern Apennines. *Boll. Soc. Geol. Ital.* **2007**, *7*, 75–112.
48. Vitale, S.; Ciarcia, S. Tectono-Stratigraphic and Kinematic Evolution of the Southern Apennines/Calabria–Peloritani Terrane System (Italy). *Tectonophysics* **2013**, *583*, 164–182. [CrossRef]
49. Vitale, S.; Ciarcia, S. Tectono-Stratigraphic Setting of the Campania Region (Southern Italy). *J. Maps* **2018**, *14*, 9–21. [CrossRef]
50. Vitale, S.; Ciarcia, S. The Dismembering of the Adria Platforms Following the Late Cretaceous-Eocene Abortive Rift: A Review of the Tectono-Stratigraphic Record in the Southern Apennines. *Int. Geol. Rev.* **2022**, *64*, 2866–2889. [CrossRef]
51. Patacca, E.; Scandone, P. Post-Tortonian Mountain Building in the Apennines. The Role of the Passive Sinking of a Relic Lithospheric Slab. *Atti Dei Convegni Lincei* **1989**, *80*, 157–176.
52. Doglioni, C.; Harabaglia, P.; Martinelli, G.; Mongelli, F.; Zito, G. A Geodynamic Model of the Southern Apennines Accretionary Prism. *Terra Nova* **1996**, *8*, 540–547. [CrossRef]
53. Improta, L.; Iannaccone, G.; Capuano, P.; Zollo, A.; Scandone, P. Inferences on the Upper Crustal Structure of Southern Apennines (Italy) from Seismic Refraction Investigations and Subsurface Data. *Tectonophysics* **2000**, *317*, 273–298. [CrossRef]
54. Ciarcia, S.; Vitale, S. Orogenic Evolution of the Northern Calabria–Southern Apennines System in the Framework of the Alpine Chains in the Central-Western Mediterranean Area. *GSA Bull.* **2024**, *137*, 1143–1176. [CrossRef]
55. Hippolyte, J.-C.; Angelier, J.; Barrier, E. Compressional and Extensional Tectonics in an Arc System: Example of the Southern Apennines. *J. Struct. Geol.* **1995**, *17*, 1725–1740. [CrossRef]
56. D'Agostino, N.; Jackson, J.A.; Dramis, F.; Funiciello, R. Interactions between Mantle Upwelling, Drainage Evolution and Active Normal Faulting: An Example from the Central Apennines (Italy). *Geophys. J. Int.* **2001**, *147*, 475–497. [CrossRef]
57. Massa, B.; Zuppetta, A. Integrated Approach to Investigation of Active Tectonics: An Example from the Calore River Fault System, Southern Italy. *Ital. J. Geosci.* **2009**, *128*, 505–513. [CrossRef]
58. Scrocca, D.; Carminati, E.; Doglioni, C. Deep Structure of the Southern Apennines, Italy: Thin-Skinned or Thick-Skinned? *Tectonics* **2005**, *24*, TC3005. [CrossRef]
59. Italiano, F.; Martelli, M.; Martinelli, G.; Nuccio, P.M. Geochemical Evidence of Melt Intrusions along Lithospheric Faults of the Southern Apennines, Italy: Geodynamic and Seismogenic Implications. *J. Geophys. Res. Solid Earth* **2000**, *105*, 13569–13578. [CrossRef]
60. De Vivo, B.; Rolandi, G.; Gans, P.B.; Calvert, A.; Bohrson, W.A.; Spera, F.J.; Belkin, H.E. New Constraints on the Pyroclastic Eruptive History of the Campanian Volcanic Plain (Italy). *Mineral. Petrol.* **2001**, *73*, 47–65. [CrossRef]
61. Barker, G.; Moscoloni, M. Ambiente e Società Nella Preistoria Dell'Italia Centrale. *NIS La Nuova Ital. Sci.* **1984**.
62. Di Bucci, D.; Massa, B.; Tornaghi, M.; Zuppetta, A. Structural Setting of the 1688 Sannio Earthquake Epicentral Area (Southern Italy) from Surface and Subsurface Data. *J. Geodyn.* **2005**, *40*, 294–315. [CrossRef]
63. Meletti, C.; Patacca, E.; Scandone, P. Construction of a Seismotectonic Model: The Case of Italy. *Pure Appl. Geophys.* **2000**, *157*, 11–35. [CrossRef]
64. CFTI5Med. Available online: https://storing.ingv.it/cfti/cfti5/ (accessed on 26 August 2025).
65. Guidoboni, E.; Ferrari, G.; Tarabusi, G.; Sgattoni, G.; Comastri, A.; Mariotti, D.; Ciuccarelli, C.; Bianchi, M.G.; Valensise, G. CFTI5Med, the New Release of the Catalogue of Strong Earthquakes in Italy and in the Mediterranean Area. *Sci. Data* **2019**, *6*, 80. [CrossRef] [PubMed]
66. Galli, P.; Galadini, F.; Pantosti, D. Twenty Years of Paleoseismology in Italy. *Earth-Sci. Rev.* **2008**, *88*, 89–117. [CrossRef]
67. Adinolfi, G.M.; De Matteis, R.; Orefice, A.; Festa, G.; Zollo, A.; de Nardis, R.; Lavecchia, G. The September 27, 2012, ML 4.1, Benevento Earthquake: A Case of Strike-Slip Faulting in Southern Apennines (Italy). *Tectonophysics* **2015**, *660*, 35–46. [CrossRef]
68. Avallone, A.; Selvaggi, G.; D'Anastasio, E.; D'Agostino, N.; Pietrantonio, G.; Riguzzi, F.; Serpelloni, E.; Anzidei, M.; Casula, G.; Cecere, G.; et al. The RING Network: Improvements to a GPS Velocity Field in the Central Mediterranean. *Ann. Geophys.* **2010**, *53*, 39–54. [CrossRef]

69. Milano, G.; Di Giovambattista, R.; Ventura, G. The 2001 Seismic Activity near Isernia (Italy): Implications for the Seismotectonics of the Central–Southern Apennines. *Tectonophysics* **2005**, *401*, 167–178. [CrossRef]
70. Mariucci, M.T.; Montone, P. Database of Italian Present-Day Stress Indicators, IPSI 1.4. *Sci. Data* **2020**, *7*, 298. [CrossRef]
71. Massa, B.; Di Bucci, D.; Tornaghi, M.E.; Zuppetta, A. Geological Survey of Quaternary Deposits in the 1688 Sannio Earthquake Epicentral Area (Benevento, Italy). *Boll. Della Soc. Geol. Ital.* **2005**, *4*, 105–117.
72. Reppert, P.M.; Morgan, F.D.; Toksöz, M.N. Dielectric Constant Determination Using Ground-Penetrating Radar Reflection Coefficients. *J. Appl. Geophys.* **2000**, *43*, 189–197. [CrossRef]
73. Hagrey, A.; Müller. GPR Study of Pore Water Content and Salinity in Sand. *Geophys. Prospect.* **2000**, *48*, 63–85. [CrossRef]
74. Goodman, D.; Piro, S.; Nishimura, Y.; Schneider, K.; Hongo, H.; Higashi, N.; Steinberg, J.; Damiata, B. Chapter 15—GPR Archaeometry. In *Ground Penetrating Radar Theory and Applications*; Jol, H.M., Ed.; Elsevier: Amsterdam, The Netherlands, 2009; pp. 479–508; ISBN 978-0-444-53348-7.
75. Annan, A.P. Chapter 1—Electromagnetic Principles of Ground Penetrating Radar. In *Ground Penetrating Radar Theory and Applications*; Jol, H.M., Ed.; Elsevier: Amsterdam, The Netherlands, 2009; pp. 1–40; ISBN 978-0-444-53348-7.
76. Slob, E.; Sato, M.; Olhoeft, G. Surface and Borehole Ground-Penetrating-Radar Developments. *Geophysics* **2010**, *75*, 75A103–75A120. [CrossRef]
77. Cassidy, N.J. A Review of Practical Numerical Modelling Methods for the Advanced Interpretation of Ground-Penetrating Radar in near-Surface Environments. *Near Surf. Geophys.* **2007**, *5*, 5–21. [CrossRef]
78. Koçak, B.; Sezgin, M.; Yeşildirek, A. Evaluation of Background Subtraction and Pattern Recognition Methods for Classification of GPR B-Scan Data. In Proceedings of the 2024 15th National Conference on Electrical and Electronics Engineering (ELECO), Bursa, Türkiye, 28–30 November 2024; pp. 1–5.
79. Shlykov, V.; Spitsyn, D.; Guzhov, S.; Tutubalin, V.; Vityazev, S.; Andreev, S.; Fan, R.; Dvorkovich, A. Signal Processing in GPR Applications for Cave-in Prediction in Road Assessment: A Review. In Proceedings of the 2025 27th International Conference on Digital Signal Processing and Its Applications (DSPA), Moscow, Russia, 26–28 March 2025; pp. 1–10.
80. Solla, M.; Lorenzo, H.; Rial, F.I.; Novo, A. Ground-Penetrating Radar for the Structural Evaluation of Masonry Bridges: Results and Interpretational Tools. *Constr. Build. Mater.* **2012**, *29*, 458–465. [CrossRef]
81. Mohapatra, S.; McMechan, G.A. Prediction and Subtraction of Coherent Noise Using a Data Driven Time Shift: A Case Study Using Field 2D and 3D GPR Data. *J. Appl. Geophys.* **2014**, *111*, 312–319. [CrossRef]
82. Crocco, L.; Ferrara, V. A Review on Ground Penetrating Radar Technology for the Detection of Buried or Trapped Victims. In Proceedings of the 2014 International Conference on Collaboration Technologies and Systems (CTS), Minneapolis, MN, USA, 19–23 May 2014; pp. 535–540.
83. Panda, S.L.; Maiti, S.; Sahoo, U.K. Subsurface Propagation Velocity Estimation Methods in Ground-Penetrating Radar: A Review. *IEEE Geosci. Remote Sens. Mag.* **2022**, *10*, 70–89. [CrossRef]
84. Smogavec, P.; Gleich, D. Surface Reflection Suppression Method for Air-Coupled SFCW GPR Systems. *Remote Sens.* **2025**, *17*, 1668. [CrossRef]
85. Zhang, B.; Cai, Y.-Q.; Yu, Z.-Y. A CNN-RNN Based Filter Model Used for Raw Tunnel Lining GPR Data. *Earthq. Res. Adv.* **2025**, *1*, 100374. [CrossRef]
86. Famiglietti, N.A.; Cecere, G.; Grasso, C.; Memmolo, A.; Vicari, A. A Test on the Potential of a Low Cost Unmanned Aerial Vehicle RTK/PPK Solution for Precision Positioning. *Sensors* **2021**, *21*, 3882. [CrossRef] [PubMed]
87. Famiglietti, N.A.; Miele, P.; Memmolo, A.; Falco, L.; Castagnozzi, A.; Moschillo, R.; Grasso, C.; Migliazza, R.; Selvaggi, G.; Vicari, A. New Concept of Smart UAS-GCP: A Tool for Precise Positioning in Remote-Sensing Applications. *Drones* **2024**, *8*, 123. [CrossRef]
88. Francke, J. A Review of Selected Ground Penetrating Radar Applications to Mineral Resource Evaluations. *J. Appl. Geophys.* **2012**, *81*, 29–37. [CrossRef]
89. Zhang, D.; Gong, H.; Li, J.; Wu, Z.; Liu, S. Integrated Ground Penetrating Radar and DGPS Method for the Continuous and Long-Distance GPR Survey in the Rugged Terrain. *Acta Geophys.* **2022**, *70*, 537–546. [CrossRef]
90. Lunina, O.V.; Gladkov, A.S.; Afonkin, A.M.; Serebryakov, E.V. Deformation Style in the Damage Zone of the Mondy Fault: GPR Evidence (Tunka Basin, Southern East Siberia). *Russ. Geol. Geophys.* **2016**, *57*, 1269–1282. [CrossRef]
91. Aliyannezhadi, A.; Mehrnia, S.R.; Kimiagar, S.; Rahimi, H.; Sadrmohammadi, N. Evaluation of GPR Method in Identification Hidden Faults of Alluvial Deposits in North of Persian Gulf Artificial Lake, Twenty-Two District of Tehran. *J. Appl. Geophys.* **2020**, *179*, 104108. [CrossRef]

Disclaimer/Publisher's Note: The statements, opinions and data contained in all publications are solely those of the individual author(s) and contributor(s) and not of MDPI and/or the editor(s). MDPI and/or the editor(s) disclaim responsibility for any injury to people or property resulting from any ideas, methods, instructions or products referred to in the content.